

Study of thermal and acoustic noise interferences in low stiffness AFM cantilevers and characterization of their dynamic properties

Mokrane Boudaoud, Yassine Haddab, Yann Le Gorrec and Philippe Lutz¹

FEMTO-ST Institute, UMR CNRS 6174 - UFC / ENSMM / UTBM Automatic Control and Micro-Mechatronic Systems Department (AS2M). 24, rue Alain Savary 25000 Besançon FRANCE.^{a)}

The Atomic Force Microscope (AFM) is a powerful tool for the measurement of forces at the micro/nano scale when calibrated cantilevers are used. Besides many existing calibration techniques, the thermal calibration is one of the simplest and fastest methods for the dynamic characterization of an AFM cantilever. This method is efficient provided that the Brownian motion (thermal noise) is the most important source of excitation during the calibration process. Otherwise, the value of the spring constant is underestimated. This paper investigates noise interference ranges in low stiffness AFM cantilevers taking into account thermal fluctuations and acoustic pressures as two main sources of noise. As a result, a preliminary knowledge about the conditions in which thermal fluctuations and acoustic pressures have closely the same effect on the AFM cantilever (noise interference) is provided with both theoretical and experimental arguments. Consequently, beyond the noise interference range, commercial low stiffness AFM cantilevers are calibrated in two ways: using the thermal noise (in a wide temperature range) and acoustic pressures generated by a loudspeaker. We then demonstrate that acoustic noises can also be used for an efficient characterization and calibration of low stiffness AFM cantilevers. The accuracy of the acoustic characterization is evaluated by comparison with results from the thermal calibration.

Keywords: Atomic Force Microscope, thermal noise, acoustic noise, micro-cantilevers, calibration process

I. INTRODUCTION

The Atomic Force Microscope (AFM) is one of the fundamental scientific instruments for high resolution surface topography at atomic scale¹, micro/nano force measurements², biological cell characterization³, chemical identification of individual surface atoms⁴, etc. Moreover, it is widely used as a manipulation tool^{5,6} at the micro and nano scale. For a measurement of the force, an accurate estimation of the spring constant (stiffness) of the AFM cantilever is crucial. Indeed, the spring constant can vary greatly from the value quoted by the manufacturers due to dimension uncertainties. Several calibration methods have been consequently reported in the literature and can be classified into three main classes: theoretical⁷, static⁸ and dynamic⁹. Some of them are presented in TABLE I. Each method is specified by the accuracy, applicability, simplicity and duration of the procedure. The calibration method to be used for a given application can be consequently defined. For instance, the nanoindentation is one of the most accurate methods, but cannot be applied on very soft cantilevers. Moreover, the dynamic added mass method is also accurate, but time consuming with a high potential damage for the cantilever.

The thermal noise method became very popular in the two last decades^{15,20-22} because of its high simplicity, ease of use and applicability to arbitrarily shaped and coated cantilevers. Moreover, this method allows the determination of the spring constant of higher modes²³.

For the fundamental mode, the first peak of the thermal spectrum is related back to the spring constant of the cantilever. Nevertheless, the accuracy of the thermal noise method depends on the resolution and the frequency bandwidth of the position measurement system (e.g. laser interferometer, photodiodes, etc.). The latter must be able to capture the overall area under the fundamental peak of the thermal spectrum for an accurate derivation of the spring constant. For this reason, the thermal method is rarely used for the calibration of stiff cantilevers (spring constant $> 1N/m$)^{8,24}. On the other hand, in low stiffness cantilevers, a major source of calibration errors stems from noises that can be misinterpreted to be thermally driven cantilever. Indeed, the thermal method can be highly inaccurate if interference with other noise sources (acoustic or mechanical noise from the environment) occurs during the characterization process leading to an underestimation of the spring constant. This issue has been raised in many publications^{18,25} and remains unanswered. Although the thermal fluctuations are often considered as a major source of noise in the AFM, studies demonstrate that acoustic noises have also an important effect on microelectromechanical systems (MEMS)^{26,27}. As such, it is important to evaluate independently the effect of acoustic and thermal noises on low stiffness AFM cantilevers and to define through models and experiments the conditions in which one of the two sources of noise is predominant to be used during a characterization process.

This paper investigates thermal and acoustic noise interferences in low stiffness AFM cantilevers. For this purpose, models are used to describe the root mean square (r.m.s) free end deflection of an AFM cantilever in response to thermal fluctuations and acoustic noises. From this modeling approach, analytical expressions of

^{a)}Electronic mail: (mokrane.boudaoud, yassine.haddab, legorrec, philippe.lutz)@femto-st.fr

TABLE I. Summary of significant aspects of the published spring constant determination technique approaches.

| Method and class | Accuracy | Ease of use | Main demerits |
|--|------------------------|-------------|--|
| Reference cantilever ^{10,11} (static) | 15 – 40% ¹² | Medium | Difficult to set one cantilever on the other accurately; both cantilevers must have spring constant values close to each other |
| Piezolever ⁸ (static) | – | Medium | Any error in the alignment of the contact piezolever/cantilever induces an inaccurate estimation of the spring constant |
| Nanoindentation ¹³ (static) | 10% ¹⁴ | Medium | The method can't be applied to very soft cantilevers ⁸ |
| Thermal noise ¹⁵ (dynamic) | 5 – 20% ¹² | High | Inaccurate if interferences with other noise sources occur during the characterization process; the need of a position sensor with a high resolution and a large frequency bandwidth |
| Sader ¹⁶ (dynamic) | 10 – 30% ¹⁷ | High | Requires a accurate knowledge of the Reynolds number of the fluid surrounding the cantilever; requires precise values of the cantilever's length, width, resonant frequency and quality factor |
| Cleveland ⁹ (dynamic) | 10 – 30% ¹⁷ | High | The length, width, resonant frequency and material properties of the cantilever must be accurately known |
| Dynamic added mass ⁹ (dynamic) | 10% ¹⁴ | Low | An accurate calibration of the added masses and point of loading are required; time consuming; high potential damage for the cantilever |
| Finite difference ⁷ , parallel beam approximation ¹⁹ (theoretical) | > 10% ¹⁸ | Medium | Requires accurate values of the cantilever dimensions and Young's modulus |

the thermal and acoustic sensitivities of the cantilever are defined. For the thermal noise, the model is derived from the equipartition theorem and for acoustic noise, the model is based on assumptions of uniform and orthogonal waves. Models are validated experimentally in a wide range of operating conditions using commercial low stiffness AFM cantilevers. A Peltier module is used for temperature variation and a specific loudspeaker is used for the acoustic characterization. As a result, a preliminary knowledge of the level of interference between such sources of noise in low stiffness cantilevers is provided. Consequently, when acoustic noises are predominant (beyond the noise interference range), we demonstrate with experiments that this source of noise can be used for an efficient characterization of the studied cantilevers based on the proposed acoustic sensitivity model. The accuracy of the acoustic characterization is evaluated by comparison with results from the thermal calibration.

II. MODELS OF THERMAL AND ACOUSTIC SENSITIVITIES OF THE AFM CANTILEVER

A. Euler Bernoulli beam equation and eigenmode decomposition

In a given environment, an AFM cantilever is subject to different sources of noise (thermal, acoustic, mechanical,...) leading to vibrations. The vibrations $z(x, t)$ along the z axis (Fig. 1) can be described by a partial differential equation using the Euler Bernoulli beam theory. For

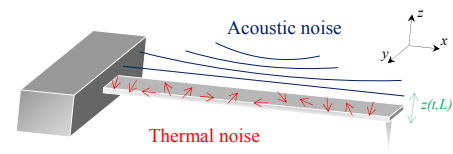


FIG. 1. Simplified scheme of an AFM cantilever subject to thermal and acoustic noises.

the case of a free undamped cantilever:

$$E.I. \frac{\partial^4 z(x, t)}{\partial x^4} + \rho.S. \frac{\partial^2 z(x, t)}{\partial t^2} = 0 \quad (1)$$

Where E is the Young's modulus, I is the second moment of inertia of the cross section, ρ is the mass density and S is the cross sectional area.

Equation (1) can be solved by the method of separation of variables (eigenfunction expansion), leading to²⁸:

$$z(x, t) = \sum_{n=1}^{\infty} \phi_n(x).e^{j.\omega_n.t} \quad (2)$$

Where $\phi_n(x)$ is a set of normalized orthogonal eigenfunctions that satisfies the following eigenequation:

$$\begin{aligned} \phi_n(x) = & (\sin(\alpha_n) + \sinh(\alpha_n)).(\cos(\frac{\alpha_n}{L}.x) - \cosh(\frac{\alpha_n}{L}.x)) \\ & - (\cos(\alpha_n) + \cosh(\alpha_n)).(\sin(\frac{\alpha_n}{L}.x) - \sinh(\frac{\alpha_n}{L}.x)) \end{aligned} \quad (3)$$

L is the length of the cantilever.

Each term in the sum of equation (2) represents a vibration mode with a frequency ω_n , and a specific constant α_n . For a cantilever structure: $\alpha_1 = 1.875$.

Considering the deflection of the free end of the cantilever ($x = L$), each vibration mode can be described as an oscillator with an effective spring constant k_{effn} and an effective mass m_{effn} , defined as²⁹:

$$k_{effn} = \frac{E.I}{\phi_n^2(L)} \cdot \int_0^L (\phi_n''(x))^2 \cdot \partial x = \frac{3.E.I}{L^3} \quad (4)$$

$$m_{effn} = \frac{\rho.S}{\phi_n^2(L)} \cdot \int_0^L \phi_n^2(x) \cdot \partial x = \frac{3}{\alpha_n^4} \cdot \rho.S.L \quad (5)$$

The dynamic equation of a vibration mode n can then be represented using a second order differential equation^{28,30}, in which a quality factor Q_n can be added to express the damping of the system:

$$m_{effn} \cdot \frac{\partial^2 z_n(t)}{\partial t^2} + \frac{m_{effn} \cdot \omega_n}{Q_n} \cdot \frac{\partial z_n(t)}{\partial t} + k_{effn} \cdot z_n(t) = F_{noise} \quad (6)$$

All external (acoustic, ground motion) and internal (thermal noise) noises are set in the F_{noise} variable.

B. Derivation of the thermal and acoustic sensitivities of the AFM cantilever

At a given temperature, the AFM cantilever is subject to random Brownian motions around an equilibrium position. Such motion is usually called thermal noise.

The thermal noise theory is derived from the equipartition theorem³¹ which states that in thermal equilibrium, the thermal energy is evenly distributed over all degrees of freedom of a given system with a mean value equal to $\frac{1}{2} \cdot K_b \cdot T$, where K_b is the Boltzman constant and T is the temperature expressed in *Kelvin*.

The Power Spectral Density (PSD) of the thermal noise at the free end of the cantilever is expressed at a vibration mode n as¹⁵:

$$S_d(f) = \frac{2 \cdot K_b \cdot T}{k_{effn} \cdot \pi \cdot f_n} \cdot \frac{Q_n}{(1 - (f/f_n)^2)^2 \cdot Q_n^2 + (f/f_n)^2} \quad (7)$$

According to this, the root mean square (r.m.s) deflection of the free end of the cantilever can be deduced for each vibration mode n by integrating the PSD in a convenient frequency interval $2\Delta f$ ³²:

$$\langle z_{thermal} \rangle_n = \sqrt{\int_{f_n - \Delta f}^{f_n + \Delta f} S_d(f) \partial f} = \sqrt{\frac{K_b \cdot T}{k_{effn}}} \quad (8)$$

We define the thermal sensitivity as the r.m.s deflection of the first vibration mode, such as:

$$\langle r.m.s_{thermal} \rangle_T = \langle z_{thermal} \rangle_1 = \sqrt{\frac{K_b \cdot T}{k_{eff1}}} \quad (9)$$

Equation (9) is also the basis of the thermal calibration method: at a given temperature T , the spring constant of an AFM cantilever k_{eff1} can be calculated by measuring the root mean square deflection of the first vibration mode from the PSD spectrum.

In addition to the thermal fluctuations, other sources of noise disturb an AFM cantilever (ground motion and acoustic noises notably). In^{33,34}, we have studied ground motion in a laboratory environment and we found it to be little significant above 350 Hz. This source of noise does not affect an AFM cantilever around its resonant frequency which is generally well above the ground motion's frequency bandwidth. However, in this work we observed that acoustic noises have a much higher effect on low stiffness micro-cantilevers. Acoustic noises are modeled as uniform and orthogonal waves.

Then, to asses the acoustic sensitivity of the AFM cantilever, we have used the static analytical expression of the cantilever deflection $z_{x_l static}$ along z axis, subject to a uniform distributed load P per unit length³⁵:

$$z_{x_l static} = \frac{P \cdot x_l^2}{24 \cdot E \cdot I} \cdot (x_l^2 - 4 \cdot L \cdot x_l + 6 \cdot L^2) \Rightarrow z_{L static} = \frac{P \cdot L^4}{8 \cdot E \cdot I} \quad (10)$$

Where x_l is the distance between a point on the cantilever and the clamped part along x axis ($0 < x_l < L$).

In dynamic mode, considering the case of an acoustic pressure W_{db} expressed in decibel relative to $20 \mu Pa$ exciting the cantilever at its first resonant mode in the z direction, equation (10) is modified to obtain the deflection at the free end of the cantilever:

$$z_{L dynamic} = \frac{20 \cdot 10^{(-6 + (W_{db}/20))} \cdot l \cdot L^4 \cdot Q_1}{8 \cdot E \cdot I} \quad (11)$$

l is the width of the cantilever.

With assumptions of linearity: in response to a sinusoidal acoustic excitation, the r.m.s deflection (i.e. acoustic sensitivity) can be obtained by dividing the maximum deflection of the free end of the cantilever $z_{L dynamic}$ by a factor of $\sqrt{2}$:

$$\langle r.m.s_{acoustic} \rangle_{W_{dB}} = \frac{20 \cdot 10^{(-6 + (W_{db}/20))} \cdot l \cdot L^4 \cdot Q_1}{8 \cdot \sqrt{2} \cdot E \cdot I} \quad (12)$$

Finally, using equation (4), we have introduced the spring constant k_{eff1} of the cantilever in equation (12), and the analytical expression of the acoustic sensitivity becomes:

$$\langle r.m.s_{acoustic} \rangle_{W_{dB}} = \frac{60 \cdot 10^{(-6 + (W_{db}/20))} \cdot l \cdot L \cdot Q_1}{8 \cdot \sqrt{2} \cdot k_{eff1}} \quad (13)$$

Equations (9) and (13) will be validated with experiments when one of the two sources of noise is predominant. After that, an interpolation of the models will be carried out for an evaluation of the noise interference range.

III. EXPERIMENTAL ANALYSIS OF THE THERMAL AND ACOUSTIC SENSITIVITIES OF THE AFM CANTILEVERS

For experiments, tipless AFM cantilevers from Mikro-Masch Inc are used: D, E and F cantilevers of the CSC12

chip (Fig. 2). The manufacturer gives typical values of the dimension, spring constant (stiffness) and resonant frequency of each cantilever as shown in TABLE II. The cantilevers are made from n-doped silicon (phosphorus doped) with a Young's modulus $E = 169\text{GPa}$.

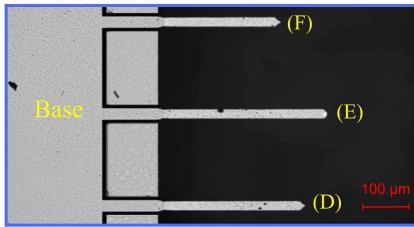


FIG. 2. F, E and D cantilevers of the CSC12 chip (Mikro-Masch Inc).

TABLE II. Dimensions, resonant frequency and stiffness (spring constant) of the F, E and D cantilevers (CSC12 chip) provided by the manufacturer. min: minimum, typ: typical, max: maximum.

| Cantilever | F | | | E | | | D | | |
|---------------------------|------|------|-----|------|------|------|------|------|-----|
| | min | typ | max | min | typ | max | min | typ | max |
| length $\pm 5\mu\text{m}$ | 250 | | | 350 | | | 300 | | |
| width $\pm 3\mu\text{m}$ | 35 | | | 35 | | | 35 | | |
| thickness | 0.7 | 1 | 1.3 | 0.7 | 1 | 1.3 | 0.7 | 1 | 1.3 |
| resonant frequency KHz | 14 | 20 | 28 | 7 | 10 | 14 | 9.5 | 14 | 19 |
| stiffness N/m | 0.02 | 0.08 | 0.2 | 0.01 | 0.03 | 0.08 | 0.01 | 0.05 | 0.1 |

The thermal sensitivity is studied in the environmental condition where most sources of acoustic noise (air conditioners, fans, etc.) are reduced. In this case, we have performed environmental acoustic measurements using a microphone (40AE) from G.R.A.S. Sound & Vibration and found that the level of acoustic noises in the frequency range [1 KHz - 20 KHz] does not exceed 15dB . Nevertheless, to ensure that in such conditions the thermal noise is predominant, the cantilevers are heated and experimental values of $\langle r.m.s_{thermal} \rangle_T$ versus the temperature are compared with the thermal noise model.

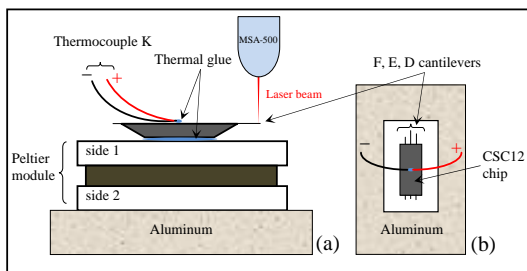


FIG. 3. Experimental setup for the thermal sensitivity analysis: side view (a) and top view (b).

On the other hand the acoustic sensitivity is studied at a constant temperature (room temperature) which

is equal to 22°C . The acoustic characterization is performed using a specific loudspeaker (see section III.B) to validate the beam deflection model based on the assumptions of uniform and orthogonal waves.

A. Analysis of the thermal sensitivity

The thermal sensitivity of the cantilevers is studied using a Peltier module from European Thermodynamics. One side of the module is attached to a heatsink made of aluminum and the CSC12 chip is glued on the other side with a thermal glue (Fig. 3). For the local temperature measurement, a type K thermocouple is fixed on the base of the chip using the thermal glue and is connected to an analog to digital converter from Texas Instruments Inc for the data acquisition.

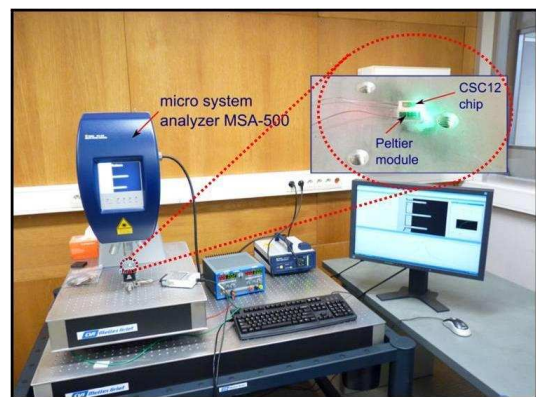


FIG. 4. Measurement of the cantilevers thermal sensitivity using the MSA-500 micro system analyzer.

The thermocouple is not attached directly to the cantilevers to avoid affecting their dynamic behavior. At a given temperature, the deflection (normal direction) at the free end of each cantilever is measured by a high resolution laser sensor (Microsystem analyzer MSA-500) from Polytec-PI Inc (Fig. 4). This device is able to perform deflection measurements at the Picometer level.

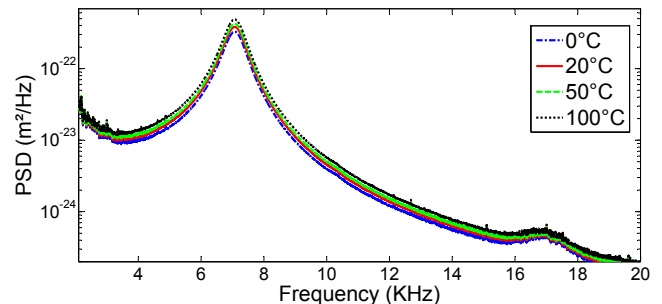


FIG. 5. Effect of the temperature on the power spectrum of the cantilever E at the first vibration mode.

The thermal sensitivity is studied according to the following steps: 1) The supply voltage of the Peltier module

is tuned in order to get a desired temperature and the CSC12 chip is maintained at this temperature during a quarter of an hour to allow a homogeneous distribution of temperature on the silicon structure. 2) Vibration measurements are performed at the free end of each cantilever with 51.2 KHZ sampling frequency. 3) The temperature is increased by $5^{\circ}C$ and steps 1 and 2 are repeated. The analysis is performed from $0^{\circ}C$ up to $100^{\circ}C$ and for each temperature, the PSD of the measured deflection is computed and averaged 128 times.

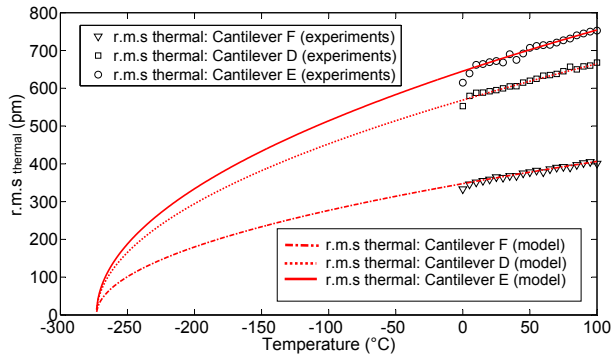


FIG. 6. Thermal sensitivity of the E, D and F cantilevers: model and experiments.

The effect of the temperature on the power spectrum of the cantilever E is shown in Fig. 5 around the first vibration mode. For studied temperatures, the resonant frequency of the cantilever remains overall constant, while the area under the fundamental peak increases with increasing temperature. This indicates that the spring constant depends very little on the temperature in the studied temperature range and that measured signals are thermal noise. The same phenomenon is observed on the two other cantilevers.

At each temperature, r.m.s deflections are calculated from PSDs in a 6 KHz bandwidth and equation (9) is fitted on obtained data using the spring constant k_{eff1} as the only parameter to be adjusted. The curve of the thermal sensitivity versus the temperature is then obtained for the three cantilevers and calibrated spring constant values are derived (see TABLE III).

A good agreement is observed between the thermal noise model (based on the equipartition theorem) and the experimental measurements (Fig. 6) when the cantilevers are well calibrated. This demonstrates that the thermal noise was predominant on the cantilevers during experiments and that the thermal sensitivity has been studied without noise interference.

B. Analysis of the acoustic sensitivity

At room temperature, the acoustic sensitivity of the cantilevers is analyzed using a loudspeaker (SD 28 CR08F) from ATOHM to generate acoustic noises, the (40 AE)

TABLE III. AFM characterization results using the thermal noise method.

| cantilever | resonant frequency | $\langle r.m.s_{thermal} \rangle_{22^{\circ}C}$ | spring constant |
|------------|--------------------|---|-----------------|
| E | 7.09 KHZ | 675pm | 0.0087N/m |
| D | 8.63 KHZ | 595pm | 0.0112N/m |
| F | 15.5 KHZ | 365pm | 0.03N/m |

microphone for acoustic measurements and a laser interferometer sensor (SP-120) from SIOS MeBTechnik GmbH for the measurement of the free end deflection of the cantilevers (Fig. 7). The loudspeaker has a large frequency bandwidth allowing the generation of acoustic noises from 1 KHz to 20 KHz. The frequency range of the microphone is [3.15 Hz - 20 KHz] and the resolution of the laser interferometer is $0.01nm$.

During the study, the microphone is placed at a 12 cm distance from the loudspeaker in order to define the acoustic level/supply voltage characteristic of the loudspeaker in the far field (Fraunhofer Region). After that, the microphone is removed and the micro-cantilevers are placed at the same distance from the loudspeaker for the analysis of the acoustic sensitivity.

The smallest wavelength λ that can generate the SD 28 CR08F loudspeaker is the one of a monochromatic acoustic signal with a frequency $f=20KHz$, such as:

$$\lambda = \frac{C}{f} = 17mm \quad (14)$$

With $C = 340m/s$ is the speed of the sound in dry air at $20^{\circ}C$.

This wavelength is 48 times larger than the length of the longest cantilever used in the study. Consequently, the hypothesis of uniform and orthogonal waves is sufficient for the acoustic sensitivity model (13).

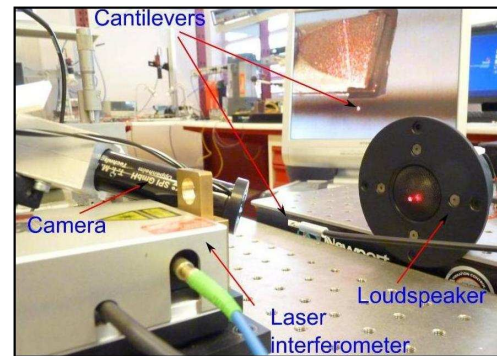


FIG. 7. Experimental setup for the acoustic sensitivity analysis.

The acoustic sensitivity is evaluated experimentally by exciting the three cantilevers (at their first resonant frequency) with sinusoidal acoustic noises from $30dB$ until $70dB$ with a step of $2dB$ between two excitations. The free end deflections of the cantilevers in response to the acoustic excitations are measured with 100 KHz sampling

TABLE IV. Acoustic and thermal sensitivities of the E, D and F cantilevers. (Values obtained from the calibrated thermal and acoustic sensitivity models)

| Cantilevers | $\langle r.m.s_{thermal} \rangle_{22^{\circ}C}$ | $\langle r.m.s_{acoustic} \rangle_{12dB}$ | $\langle r.m.s_{acoustic} \rangle_{24dB}$ | $\langle r.m.s_{acoustic} \rangle_{60dB}$ |
|-------------|---|---|---|---|
| E | 675pm | 331.11pm | 1.31nm | 83nm |
| D | 595pm | 296.33pm | 1.17nm | 74.43nm |
| F | 365pm | 215.17pm | 856.63pm | 54.05nm |

frequency. Then, experimental $\langle r.m.s_{acoustic} \rangle_{W_{dB}}$ are obtained according to the level of acoustic noises.

To avoid the transmission of the vibrations caused by the loudspeaker to the cantilevers through the ground, the support holding the cantilevers is fixed on a vibration isolation table while the loudspeaker is positioned out of this table.

The measurements of the deflections of the free end of the cantilevers by the laser sensor are performed in two conditions: -in the first one, the head of the laser sensor is placed at a 50mm distance from the cantilevers, - in the second one, the distance is increased by 190mm. For the two conditions, the difference between the amplitude of the deflection of the cantilevers during the acoustic excitation, is found to be less than 1%. This comparison is performed to check if acoustic waves are reflected back to the cantilevers due to the head of the laser sensor.

The acoustic sensitivity model (13) is then compared with the experimental r.m.s measurements using the ratio Q_1/k_{eff1} as the only parameters to be adjusted. The typical values of the length L and the width l given by the manufacturer (see TABLE II) are used in the model.

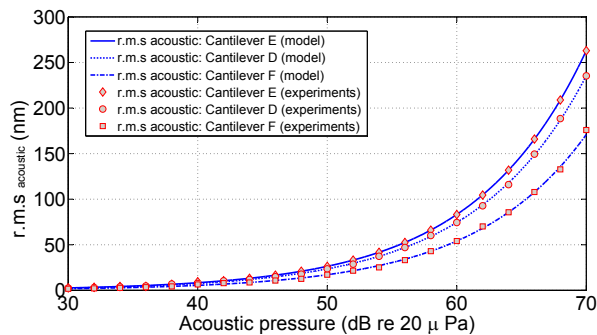


FIG. 8. Acoustic sensitivity of the E, D and F cantilevers: model and experiments.

The good agreement between the model and the experimental r.m.s measurements (Fig. 8) is obtained for ratios equal to: 1.28×10^3 , 1.33×10^3 and 1.16×10^3 for the cantilevers E, D and F respectively. Results of the characterization show the high sensitivity of the cantilevers to acoustic noises and that for the range of acoustic pressures produced by the loudspeaker, the thermal noise is exceeded.

The thermal and acoustic sensitivity models have been validated with experiments when one of the two sources of noise is predominant. However, in the noise inter-

ference range it is not possible to evaluate experimentally the contribution of each source of noise on the r.m.s deflection. To overcome this limitation, the calibrated models are used to describe separately the effect of each source of noise on the cantilevers when both noises are significant.

C. Analysis of the noise interference range

The range of interference between the two studied sources of noise is analyzed by comparing the thermal and acoustic sensitivity models of each cantilever. In the case of the cantilever E, Fig. 9 shows the two curves of interest.

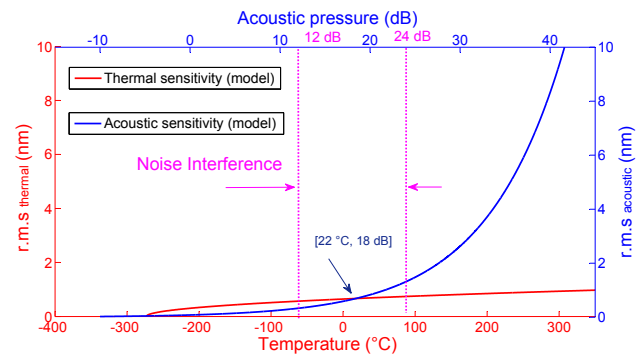


FIG. 9. Acoustic and thermal sensitivities of the cantilever E: derivation of the noise interference range.

At room temperature, the level of the r.m.s thermal noise is closely the same than the r.m.s deflection produced with 18dB acoustic noises. In this environmental condition, the interference between the two sources of noise is maximum and no efficient characterization process can be performed. Moreover, by referring to the acoustic sensitivity model, at 12dB, 50% of the thermal noise is reached and for 24dB the thermal noise is surpassed only by a factor of 2 (see TABLE IV). We have then defined the range of the noise interference at room temperature to be [12dB – 24dB] for the cantilever E. The same work has been performed for the two other cantilevers and the noise interference range at room temperature is obtained for the following acoustic levels: [13dB – 25dB] and [16dB – 28dB] for cantilevers D and F respectively. Note that, the analysis of the noise interference range can also be performed considering a temperature range and a constant acoustic pressure.

The noise interference range for the three cantilevers is shown in Fig. 10. Such results provide a knowledge on the order of magnitude of acoustic noises which produce a high interference with thermal fluctuations in cantilevers whose spring constants are close to ones of the studied AFM cantilevers. Environments in which atomic force microscopes operate are often noisy. The sources of noise are typically heating and cooling vents, laboratory fume hoods, external traffic, etc. The study reported in this paper demonstrates the influence of such environments on low stiffness AFM cantilevers when the level of the acoustic noise exceeds 30dB at the [1 KHz - 20 KHz] frequency range. Environmental conditions in which an acoustic isolation platform is required can then be defined.

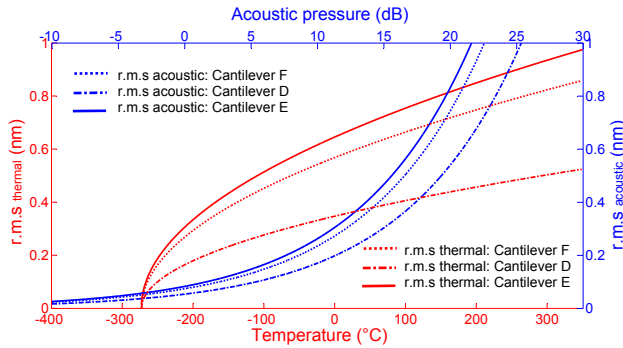


FIG. 10. Enlarged view of noise interferences in the cantilevers E, D and F.

In this study, we consider that acoustic noises can also be advantageously used for the characterization of an AFM cantilever when the threshold of the thermal noise is exceeded (see Fig. 9). Indeed, acoustic noises can generate r.m.s deflections with magnitudes reaching several nanometers if the cantilever is excited at its first resonant frequency. Then, the experimental derivation of the cantilever resonant frequency, the quality factor and the spring constant values can be performed without the use of position sensors with a Picometer resolution. In the next section, we demonstrate experimentally the effectiveness of such a characterization process. For this purpose, the knowledge of the noise interference range is fundamental for an appropriate choice of the level (magnitude) of acoustic noises required for the characterization.

IV. CHARACTERIZATION OF THE AFM CANTILEVERS USING ACOUSTIC NOISE

In this section, a calculation of the cantilevers resonant frequency is performed in the time domain, the spring constant and the quality factor are identified from experimental deflection measurement and the accuracy of the identified parameters is evaluated.

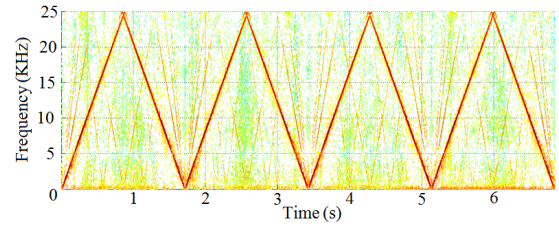


FIG. 11. Spectrogram of the chirp signal measured by the 40 AE microphone.

A. Estimation of the cantilevers resonant frequency

The precise value of the resonant frequency of an AFM cantilever is required in many existing calibration techniques such as the Cleveland method and the Sader method (see TABLE I). We propose to estimate the resonant frequency of the cantilevers without the use of a spectral analysis. Indeed, in the frequency domain, the precise value of the resonant frequency is quite difficult to obtain due to the low quality factor of the cantilevers.

A frequency sweep is then performed to estimate the frequency which causes the largest deflection of the cantilever. A linear chirp signal is then generated. The general equation of this signal is:

$$Chirp(t) = \sin\left(2\pi.\left(f_0 + \frac{f_1 - f_0}{t_1}.t\right).t\right) \quad (15)$$

Where f_0 and f_1 are the instantaneous frequencies at times $t = 0$ and $t = t_1$ respectively.

When generating a discrete linear chirp signal with a sampling frequency F_e , the frequency sweep occurs from f_0 at $t = 0$ until $\frac{F_e}{2}$ at $t = t_{F_e}$ with a positive slope when $0 < t < t_{F_e}$ and a negative slope for $t_{F_e} \leq t < 2t_{F_e}$. The frequency sweep is then repeated with a period of $2.t_{F_e}$. This can be observed through the spectrogram of the chirp signal.

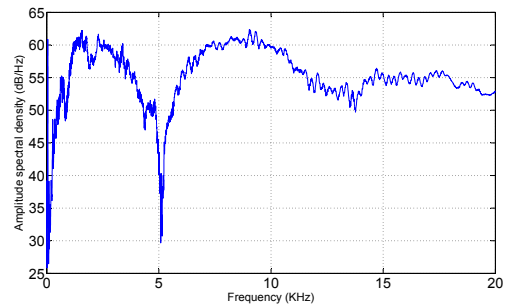


FIG. 12. Amplitude spectral density of the chirp signal.

In our study, a discrete linear chirp signal is generated with 50 KHz sampling frequency. The parameters of the signal are defined as: $f_0 = 1$ Hz, $f_1 = 15$ KHz and $t_1 = 0.5$ s. The spectrogram and the amplitude spectral density of this acoustic signal measured by the microphone are shown in Fig. 11 and Fig. 12 respectively.

TABLE V. Comparison between the characterization results of the E, D and F cantilevers using the thermal and acoustic approaches.

| Cantilever | Thermal noise method | | | acoustic noise method | | | error | | |
|------------|----------------------|-------------|-------|-----------------------|-------------|-------|-----------|-----------------|-----------|
| | f_1 | k_{eff_1} | Q_1 | f_1 | k_{eff_1} | Q_1 | f_1 (%) | k_{eff_1} (%) | Q_1 (%) |
| E | 7.09 KHz | 0.0087N/m | 9.5 | 7.069 KHz | 0.0076N/m | 9.73 | 0.29% | 12.64% | 2.42% |
| D | 8.63 KHz | 0.0112N/m | 12.25 | 8.96 KHz | 0.0098N/m | 13.1 | 3.82% | 12.5% | 6.93% |
| F | 15.5 KHz | 0.03N/m | 19.1 | 15.7 KHz | 0.0176N/m | 20.5 | 1.29% | 41.33% | 7.32% |

The three studied AFM cantilevers are excited with the same chirp signal and the resulting free end deflections are measured with the SP-120 laser interferometer sensor. The maximum deflection of the cantilevers is obtained at precise time intervals: ΔTE , ΔTD and ΔTF for the cantilevers E, D and F respectively (Fig. 13). Each time interval is related to the resonant frequency which can be extracted from the spectrogram of the chirp signal. According to this, a precise value of the first flexural resonant frequency is obtained for each cantilever (TABLE V). Results are compared with ones derived from the thermal spectrum.

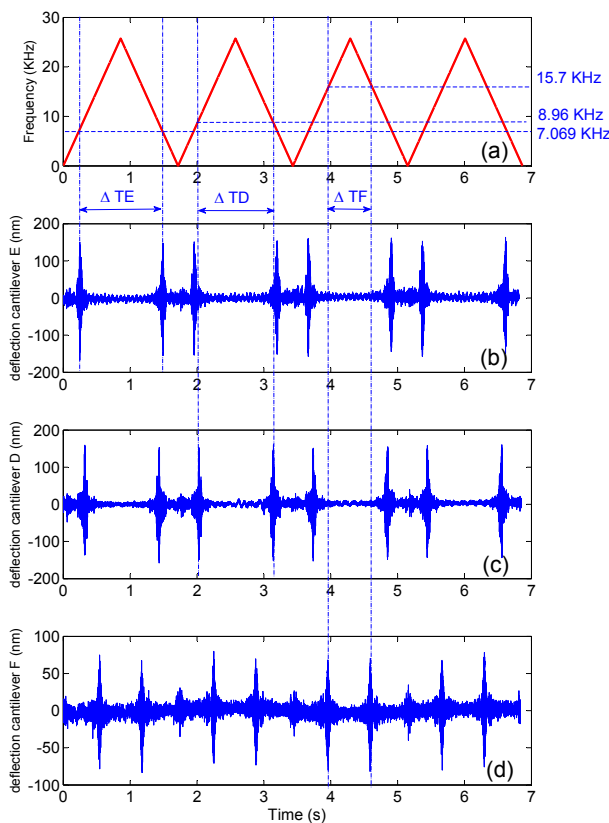


FIG. 13. Characterization of the first resonant frequency of the AFM cantilevers using the acoustic chirp signal. Spectrogram of the chirp signal (a), free end deflection of the cantilevers E (b), D (c) and F (d).

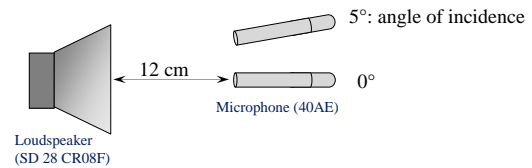


FIG. 14. Simplified scheme showing the position of the microphone according to two different angles of incidence.

B. Identification of the spring constant and the quality factor

The ratio Q_1/k_{eff_1} of each cantilever has been estimated in section III. B using the acoustic sensitivity model in which the length and the width of each cantilever are taken as provided by the manufacturer (typical values).

It must be noted that one of the major source of uncertainty in the estimation of the ratio Q_1/k_{eff_1} stems from the acoustic noise measurement error. For instance, at 60dB, a measurement error of 1dB leads to an uncertainty of 12.2% in equation (13). This uncertainty is equal to 18.85% if the measurement error is 1.5dB. The error in the acoustic noise measurement is mostly due to the angle of incidence (Fig. 14) between the microphone and the loudspeaker.

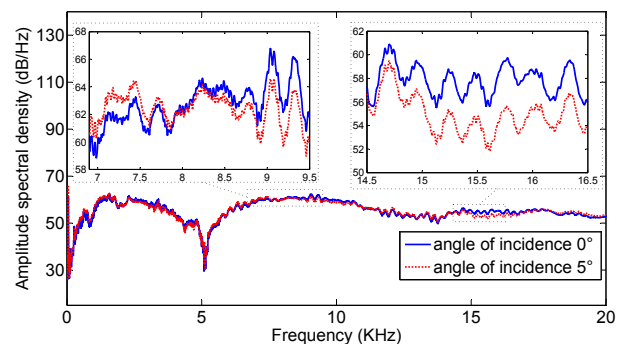


FIG. 15. Effect of the angle of incidence on the amplitude spectral density of the chirp signal measured by the 40 AE microphone.

As such, Fig. 15 shows the effect of a deviation of 5° of the angle of incidence on the amplitude spectral density of the chirp signal previously generated. The level of the measurement's error at frequencies neighboring the resonant frequencies of the studied cantilevers can be ob-

served. For this reason, throughout the study, a fine adjustment of the angle of incidence has been performed before each acoustic noise measurement.

On the other hand, the accuracy of the acoustic calibration method can be improved if the length and the width of each cantilever are measured under a Scanning Electron Microscope (SEM). Indeed, uncertainties of the length are 1.42%, 1.66% and 2% for the cantilevers E, D and F respectively. Besides, the uncertainty of the width is much higher and equal 10.57% for all the cantilevers. Such improvement will be carried on in future works.

To identify separately the spring constant and the quality factor of the cantilevers, we have used the second order differential equation described in equation (6) considering the first vibration mode (i.e. $n = 1$) and the acoustic sensitivity model to obtain the following equation:

$$\frac{\partial^2 z_1(t)}{\partial t^2} + \frac{\omega_1}{Q_1} \cdot \frac{\partial z_1(t)}{\partial t} + \frac{k_{eff1}}{m_{eff1}} \cdot z_1(t) = \frac{F_{noise}}{m_{eff1}} \quad (16)$$

With:

$$F_{noise} = \frac{60.10^{(-6+(W_{db}/20))} \cdot L}{8} \quad (17)$$

In order to reduce the number of parameters to be identified, the effective mass is expressed in terms of the effective spring constant and the angular frequency of the first vibration mode:

$$\frac{\partial^2 z_1(t)}{\partial t^2} + \frac{\omega_1}{Q_1} \cdot \frac{\partial z_1(t)}{\partial t} + \omega_1^2 \cdot z_1(t) = \frac{\omega_1^2}{k_{eff1}} \cdot F_{noise} \quad (18)$$

Then, the model is translated into the state space representation. The free end deflection z_1 and the velocity \dot{z}_1 are the states of the model:

$$\begin{bmatrix} \dot{z}_1 \\ \ddot{z}_1 \end{bmatrix} = \begin{bmatrix} 0 & 1 \\ -\omega_1^2 & -\frac{\omega_1}{Q_1} \end{bmatrix} \cdot \begin{bmatrix} z_1 \\ \dot{z}_1 \end{bmatrix} + \begin{bmatrix} 0 \\ \frac{\omega_1^2}{k_{eff1}} \end{bmatrix} \cdot F_{noise} \quad (19)$$

$$z = \begin{bmatrix} 1 & 0 \end{bmatrix} \cdot \begin{bmatrix} z_1 \\ \dot{z}_1 \end{bmatrix}$$

In this study, since the ratio Q_1/k_{eff1} is known (see section III.B), the only parameter to be identified is the quality factor Q_1 . The angular frequency (proportional to the resonant frequency) has been accurately estimated with the acoustic characterization. Moreover, the spring constant can be thereafter deduced from the identified quality factor and the ratio Q_1/k_{eff1} .

For the identification, a sinusoidal acoustic noise of a magnitude equal to 60dB is generated by the loudspeaker. This magnitude is chosen to ensure that the experiments are performed well above the noise interference range. The purpose is to excite the cantilever at its first resonant frequency. Then, the free end deflection is measured with the laser interferometer sensor (SP-120).

In the model, a sinusoidal signal is set in the variable F_{noise} with $W_{db} = 60dB$. The frequency of the signal is equal to the resonant frequency of the cantilever to

be characterized. To solve equation (19), several solvers from the Matlab software have been tested (ode45, ode23, ode113 and ode23s). We found that the most accurate solution (comparing to the experimental deflection measurement) is obtained with the ode23s solver which is well adapted to problems with crude error tolerances.

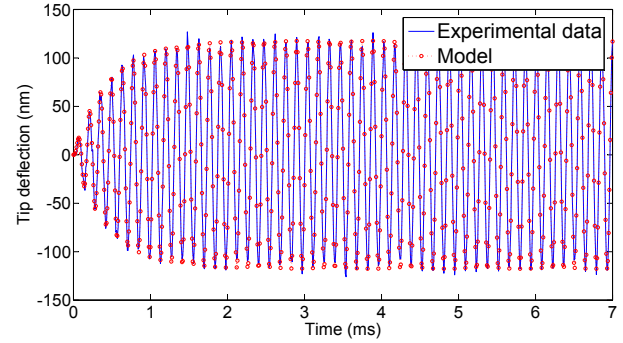


FIG. 16. Free end deflection of the cantilever E in response to a 60dB sinusoidal excitation at its first resonant frequency (model and experimental measurements).

The value of Q_1 within the model is then optimized using the experimental data and a least squares identification method (Levenberg- Marquardt algorithm). Starting from an initial value of the parameter to be optimized as: $Q_1 = 500$, the optimal value leading to a minimum error between the output of the model and the experimental deflection (Fig. 16) is obtained for each cantilever and results are presented in TABLE V. The maximum error in the estimation of the quality factor between the thermal and acoustic methods is less than 8%. For the thermal method, the quality factor is derived by fitting equation (7) on the thermal spectrum at room temperature.

Moreover, the values of the spring constant of each cantilever are deduced and compared with ones calibrated from the thermal method. Results are also reported in TABLE V. The estimation of the spring constant with the acoustic method leads to a maximum error (taking into account the thermal calibration as a reference) of 41.33% for the case of the cantilever F.

The acoustic characterization method can be extended to the analysis and the characterization of stiffer cantilevers provided that the scientific instrumentation for the acoustic noise analysis is characterized by a frequency bandwidth covering the first resonant frequency of the AFM cantilever. Some commercially available microphones and loudspeakers can cover frequency bandwidths from several Hz up to 100 KHz. For instance the 40BF microphone from G.R.A.S. Sound & Vibration has a frequency range of [10 Hz - 100 KHz]. Moreover, the ESTD01 sound generator designed by Murata Manufacturing Company, Ltd. is characterized by a frequency bandwidth of [15 KHz - 100 KHz].

V. SUMMARY AND CONCLUSIONS

In this paper, thermal and acoustic noises in low stiffness AFM cantilevers have been analyzed. Models and experiments allowed defining independently the contribution of each source of noise on the r.m.s free end deflection of three different commercial low stiffness AFM cantilevers. The purpose has been to evaluate the conditions in which acoustic and thermal noises are uncorrelated to be used during a dynamic characterization process. To this end, the thermal noise model derived from the equipartition theorem has been verified experimentally in a wide temperature range in low acoustic noise conditions. Moreover, the acoustic sensitivity of the cantilevers has been studied at room temperature using a specific scientific instrumentation and experiments have been compared with a model. Results allowed the determination of level of interference between such sources of noise in low stiffness cantilevers. Consequently, the level of acoustic noises required to generate r.m.s free end deflections exceeding the noise interference range is defined. In this case, the potential of using acoustic noises for the characterization of low stiffness AFM cantilevers is demonstrated through experimental results. The accuracy of the acoustic characterization is evaluated by comparison with results from the thermal calibration. Acoustic noise allows a fast easy and nondestructive estimation of the resonant frequency, the spring constant and quality factor of an AFM cantilever. Moreover this method can be used as a complement tool aiming at improving the accuracy of some existing calibration methods.

ACKNOWLEDGMENTS

The authors would like to thank Patrick ROUGEOT for helpful discussions about the calibration and the characterization of AFM cantilevers.

¹Y. Song, and B. Bhushan, *Phys. Rev. B.* **74**, 165401 (2006).

²D. Bachmann, and C. Hierold, *J. Micromech. Microeng.* **17**, 102 (2007).

³A. Trache, J. P. Trzeciakowski, L. Gardiner, Z. Sun, M. Muthuchamy, M. Guo, S. Y. Yuan, and G. A. Meininger, *Biophysical Journal.* **89**, 2888 (2005).

⁴Y. Sugimoto, P. Pou, M. Abe, P. Jelinek, R. Perez, S. Morita, and O. Custance,

⁵M. Sitti, and H. Hashimoto, *IEEE/ASME transactions on mechatronics.* **5**, 199 (2000).

⁶H. Xie and S. Regnier, *Rev Sci Instrum.* **81**, 035112 (2010).

⁷J. M. Neumeister and W. A. Ducker, *Rev Sci Instrum.* **65**, 2527 (1994).

⁸S. B. Aksu, and J. A. Turner, *Rev Sci Instrum.* **78**, 43704 (2007).

⁹J. P. Cleveland, S. Manne, D. Bocek, and P. K. Hansma, *Rev Sci Instrum.* **64**, 403 (1993).

¹⁰A. Torii, M. Sasaki, K. Hane, and S. Okuma, *Meas. Sci. Technol.* **7**, 179 (1996).

¹¹C. T. Gibson, G. S. Watson, and S. Myhra, *Nanotechnology.* **7**, 259 (1996).

¹²I. Chasiotis, *Springer Handbook of Experimental Solid Mechanics, Part B*, 409-444, DOI: 10.1007/978-0-387-30877-7, (2008)

¹³J. D. Holbery, and V. L. Eden, *J. Micromech. Microeng.* **10**, 85 (2000).

¹⁴J. D. Holbery, V. L. Eden, M. Sarikaya, and R. M. Fisher, *Rev Sci Instrum.* **71**, 3769 (2000).

¹⁵G. A. Matei, E. J. Thoreson, J. R. Pratt, D. B. Newell, and N. A. Burnham, *Rev Sci Instrum.* **77**, 083703 (2006).

¹⁶J. E. Sader, J. W. M. Chon, and P. Mulvaney, *Rev Sci Instrum.* **70**, 3967 (1999).

¹⁷C. T. Gibson, D. A. Smith, and C. J. Roberts, *Nanotechnology.* **16**, 234 (2005).

¹⁸P. J. Cumpson, P. Zhdan, and J. Hedley, *Ultramicroscopy.* **100**, 241 (2004).

¹⁹T. J. Senden, and W. A. Duckert, *Langmuir.* **10**, 1003 (1994).

²⁰J. L. Hutter, and J. Bechhoefer, *Rev Sci Instrum.* **64**, 1868 (1993).

²¹N. A. Burnham, X. Chen, C. S. Hodges, G. A. Matei, E. J. Thoreson, C. J. Roberts, M. C. Davies, and S. J. B. Tendler, *Nanotechnology.* **14**, 1 (2003).

²²C. T. Gibson, B. L. Weeks, J. R. I. Lee, C. Abell, and T. Rayment, *Rev Sci Instrum.* **72**, 2340 (2001).

²³J. R. Lozano, D. Kiracofe, J. Melcher, R. Garcia, and A. Raman, *Nanotechnology.* **21**, 465502 (2010).

²⁴B. W. Hoogenboom, P. L. T. M. Frederix, D. Fotiadis, H. J. Hug, and A. Engel, *Nanotechnology.* **19**, 384019 (2008).

²⁵S. J. Kennedy, D. G. Cole, and R. L. Clark, *Rev Sci Instrum.* **80**, 125103 (2009).

²⁶R. N. Dean, G. T. Flowers, A. S. Hodel, G. Roth, S. Castro, R. Zhou, A. Moreira, A. Ahmed, R. Rifki, B. E. Grantham, D. Bittle, J. Brunsch, *IEEE International Symposium on Industrial Electronics*, Vigo, 2007.

²⁷R. N. Dean, G. T. Flowers, A. S. Hodel, K. Macallister, R. Horvath, A. Matras, R. Glover, *International conference on advanced packaging and systems*, Reno NV, 2002.

²⁸J. R. Lozano, and R. Garcia, *Phys. Rev. B.* **79**, 014110 (2009).

²⁹M. V. Salapaka, H. S. Bergh, J. Lai, A. Majumdar, and E. McFarland, *J. Appl. Phys.* **81**, 2480 (1997).

³⁰J. Melcher, S. Hu, and A. Raman, *Appl. Phys. Lett.* **91**, 053101 (2007).

³¹H. J. Butt, and M. Jaschke, *Nanotechnology.* **6**, 1 (1995).

³²P. Paolino, B. Tiribilli, and L. Bellon, *Journal of Applied Physics.* **106**, 094313 (2009).

³³M. Boudaoud, Y. Haddab, Y. Le Gorrec, and P. Lutz, *Proceedings of the IEEE International Conference on Robotics and Automation*, Shanghai, 2011.

³⁴M. Boudaoud, Y. Haddab, Y. Le Gorrec, and P. Lutz, *Mechatronics journal.* **21**, 1087 (2011).

³⁵J. M. Gere, and S. P. Timoshenko, *Mechanics of Materials*, PWS Publishing Company, 1997.